PERGAMON

International Journal of Solids and Structures 39 (2002) 41–63

INTERNATIONAL JOURNAL OF SOLIDS and STRUCTURES

www.elsevier.com/locate/ijsolstr

Modeling of joints with clearance in flexible multibody systems

Olivier A. Bauchau *, Jesus Rodriguez

School of Aerospace Engineering, Georgia Institute of Technology, 270 Ferst Drive, Atlanta, GA 30332-0150, USA

Received 22 February 2001; in revised form 24 July 2001

Abstract

This paper is concerned with the modeling of joints with clearance within the framework of finite element based dynamic analysis of nonlinear, flexible multibody systems. For actual joints, clearance, lubrication and friction phenomena can significantly affect the dynamic response of the system. In this work, the effects of clearance and lubrication are studied for revolute and spherical joints. The formulation is developed within the framework of energy preserving and decaying time integration schemes that provide unconditional stability for nonlinear, flexible multibody systems. Numerical examples are presented that demonstrate the efficiency and accuracy of the proposed approach. The importance of modeling structural damping and limited driving power are discussed.

Keywords: Clearance; Joints; Multibody dynamics; Lubrication

1. Introduction

Joints are essential components of multibody systems, rigid or flexible. Usually, joints are modeled as perfect components; in fact, in most multibody formulations, joints are not modeled per se. Rather, the effect of joints, i.e. the constraints they impose on the behavior of the entire system, are modeled through a set of kinematic constraints; the piece of hardware that actually constitutes the joint is not modeled. In actual joints, clearance, friction, lubrication and impact forces will play an important role and can have a significant effect on the dynamic response of the system. For instance, impact forces due to clearance induce increased vibration and noise, reduce component life, and result in a loss of precision. Conversely, wear, imperfections and tolerance mismatches result in joint clearances. Consequently, proper modeling of these effects is required to achieve a better understanding of the phenomena associated with these imperfections.

There is a significant amount of literature discussing the treatment of clearance in joints. A variety of problems have been considered: systems with rigid or flexible linkages presenting planar or spatial configurations. Furthermore, a number of tribology effects have been investigated: friction, wear, and

* Corresponding author. Fax: +1-404-894-2760.
E-mail address: olivier.bauchau@ae.gatech.edu (O.A. Bauchau).

0020-7683/01/$ - see front matter
PII: S0020-7683(01)00186-X

lubrication of the interacting surfaces. Although many of these effects have been studied individually, very few formulations present comprehensive models for predicting the dynamic response of flexible multibody systems with joint clearance.

A paper by Haines (1980) reviews the literature concerned with planar motion and impact at revolute joints. Several authors have focused on systems with rigid links (see e.g. Rogers and Andrews, 1977; Bengisu et al., 1986; Rhee and Akay, 1996; Zakhariev, 1999); however, this assumption seems to be too restrictive for many practical systems. Consequently, flexibility effects were added in many subsequent investigations. Dubowsky et al. (1987), Deck and Dubowsky (1994) considered the effect of link flexibility for both planar and spatial cases but ignored the effect of lubrication. Liu and Lin (1990) added lubrication effects through the squeeze film formula and Reynolds equation, although his formulation was limited to planar problems. Xie et al. (1999) discuss the effect of joint clearance in planar problems without treating the effect of lubrication. Bifurcation diagrams were used as a tool to examine system dynamic behavior. Ravn et al. (1999) studied the effect of clearance on system response, including the effect of lubrication and link flexibility. However, their model was limited to planar problems. All these papers focused on the modeling of clearance in joints. Various formulations were used to model the multibody system and the linkages were modeled as rigid components, or elastic components with modal reduction.

At the heart of the formulation of models for joints with clearance is the simulation of intermittent contact. The different approaches to model intermittent contact fall into two broad categories depending on the assumed duration of contact. In the first approach, contact is treated as a discontinuity, i.e. the duration of contact is assumed to tend to zero. The configuration of the system is assumed to be identical before and after impact, and the principle of impulse and momentum is used to compute the momenta after impact. Energy transfer during impact can be modeled in a heuristic manner using the concept of coefficient of restitution. This approach was first proposed by Kane (1962) , then applied to rigid multibody systems by Haug et al. (1981), and extended to flexible systems by Khulief and Shabana (1986). The accuracy of this approach is inherently limited by the assumption of a vanishing impact duration. Furthermore, energy balance is not necessarily satisfied when the principle of impulse and momentum is applied (Kane, 1968).

In the second approach to contact modeling, the impact duration is finite, and the time history of the forces acting between the contacting bodies which can be either rigid or deformable is explicitly computed during the simulation. Of course, a constitutive law describing the force–deformation relationship for the contacting bodies is required if the bodies are deformable. This approach was used by a number of researchers Khulief and Shabana (1987), Lankarani and Nikravesh (1990), Cardona and Géradin (1993), among others. Various types of constitutive laws were used, but the classical solution of the static contact problem presented by Hertz, (see e.g. Timoshenko and Gere, 1961), has been used by many investigators. Energy dissipation can be added in an appropriate manner, as proposed by Hunt and Crossley (1975).

In the present formulation, elastic bodies are modeled using the finite element method. For beam elements, the location of each node is represented by its Cartesian coordinates in an inertial frame, and the rotation of the cross-section at each node is represented by a finite rotation tensor expressed in the same inertial frame. The kinematic constraints among the various bodies are enforced via the Lagrange multiplier technique. Although this approach does not involve a minimum set of coordinates, it allows a modular development of finite elements for the enforcement of the kinematic constraints.

The modeling of joints with clearance is divided in three distinct parts: (1) a purely kinematic part describing the configuration of the joint inner and outer races, (2) a unilateral contact condition giving rise to a contact force and (3) a lubrication model.

Section 3 describes the kinematic aspects of the problem for both two- and three-dimensional configurations. The candidate contact points (see e.g. Pfeiffer and Glocker (1996)) i.e. the points on the inner and outer races that are about to come in contact, are obtained from relatively simple geometric considerations and the definition of the relative distance q between the races follows.

The second part of the model, described in Section 4, is the unilateral contact condition which is readily expressed in terms of the relative distance as $q \geqslant 0$. This contact condition can be represented as a purely kinematic condition $q - r^2 = 0$, where r is a slack variable used to enforce the positiveness of q. In order to accommodate for the local deformation of the races, the local penetration or *approach*, denoted a, is defined, and the contact condition then writes $q + a - r^2 = 0$. The last part of the model, presented in Section 5, deals with the forces associated with a thin oil film present between the inner and outer races of the joints. A closed form solution of Reynolds equation is used for this purpose.

In the last section, numerical examples are presented that demonstrate the versatility and efficiency of proposed model. The effects of structural damping and limited driving power are discussed.

The discretization of the various components of this model were formulated within the framework of the energy preserving (see e.g. Simo and Wong, 1991; Simo et al., 1995; Simo and Tarnow, 1994; Simo and Tarnow, 1992; Bauchau et al., 1995) and decaying schemes (see e.g. Bauchau and Theron, 1996a,b; Bottasso and Borri, 1997; Bottasso and Borri, 1998; Bauchau and Joo, 1999; Bauchau, 1998; Bottasso et al., 2000; Bauchau and Bottasso, 1999). In these schemes, unconditional stability is achieved for nonlinear elastic multibody systems by combining two features: an energy preservation or decay statement for the elastic bodies of the system, and the vanishing of the work done by the forces of constraint. The use of these unconditionally stable schemes is of particular importance in problems involving joints with clearance, due to the presence of a number of nonlinear holonomic constraints, and to the rapidly varying dynamic response of the system associated with the intermittent contact phenomena.

2. Kinematic conventions and notations

The kinematic description of bodies in their reference and deformed configurations will make use of three orthogonal triads. First, an inertial triad is used as a global reference for the system; it is denoted $\mathscr{S}_I$ with unit vectors $\mathbf{i}_1$, $\mathbf{i}_2$, and $\mathbf{i}_3$. A second triad $\mathscr{S}_0$, with unit vectors $\mathbf{e}_{01}$, $\mathbf{e}_{02}$, and $\mathbf{e}_{03}$ is attached to the body and defines its orientation in the reference configuration. Finally, a third triad $\mathscr{S}^*$ with unit vectors $\mathbf{e}_1$, $\mathbf{e}_2$, and $\mathbf{e}_3$ defines the orientation of the body in its deformed configuration.

Let $\mathbf{u}_0$ and $\mathbf{u}$ be the displacement vectors from $\mathscr{S}_I$ to $\mathscr{S}_0$, and $\mathscr{S}_0$ to $\mathscr{S}^*$, respectively, and $\mathbf{R}_0$ and $\mathbf{R}$ the rotation tensors from $\mathscr{S}_I$ to $\mathscr{S}_0$, and $\mathscr{S}_0$ to $\mathscr{S}^*$, respectively. In this work, all vector and tensor components are measured in either $\mathscr{S}_I$ or $\mathscr{S}^*$. For instance, the components of vector $\mathbf{u}$ measured in $\mathscr{S}_I$, and $\mathscr{S}^*$ will be denoted $\underline{u}$, and $\underline{u}^*$, respectively, and clearly

$$\underline{u}^* = R_0^{\mathrm{T}} R^{\mathrm{T}} \underline{u}. \tag{1}$$

Similarly, the components of tensor $\mathbf{R}$ measured $\mathscr{S}_I$, and $\mathscr{S}^*$ will be denoted R, and R^*, respectively. The skew-symmetric matrix formed with the components $\underline{u}$ will be denoted $\widetilde{u}$.

3. Kinematic description of joints with clearance

The kinematic description of joints with clearance will be divided into two- and three-dimensional models. For two-dimensional problems, a revolute joint with clearance can be viewed as a planar joint with a unilateral constraint (see Section 3.1). The clearance, or distance between the inner and outer races, can be evaluated from the kinematic variables associated with the planar joint. A similar approach can be applied to spherical joints with clearance. In the three-dimensional case, the clearance can still be related to the kinematic variables of the joint, although this relationship is more complex (see Section 3.2).

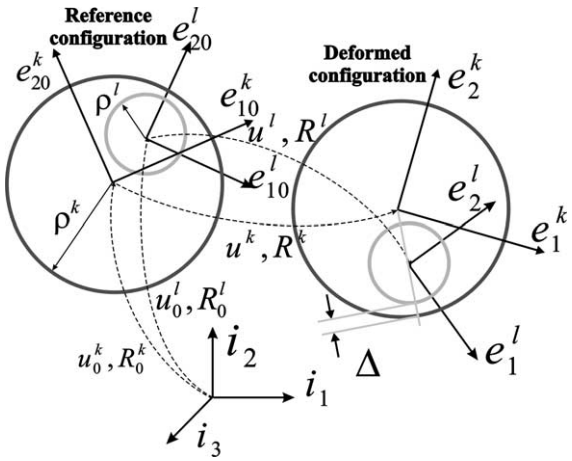

Fig. 1. Planar joint in the reference and deformed configurations.

3.1. Two-dimensional case: the planar clearance joint

A revolute joint with clearance can be modeled as a planar joint with the appropriate addition of a unilateral contact condition. Consider the planar joint depicted in Fig. 1; the outer and inner races of the joint are modeled as bodies K and L, respectively. In the reference configuration, the position of body K is defined by its position vector $\underline{u}^k_0$ and its orientation is determined by a body attached triad $\mathscr{S}^k_0$, with $\underline{e}^k_{30}$ normal to the plane of joint. The radius of the outer race is denoted ρ^k. In the deformed configuration, body K undergoes a displacement $\underline{u}^k$ and its orientation is defined by a triad $\mathscr{S}^k$. The kinematic variables associated with body L, which represents the inner race of the revolute joint, are defined in a similar manner.

The planar joint is associated with the following constraint conditions

$$\mathscr{C}_1 = \underline{e}^{l\mathrm{T}}_1 \underline{e}^k_3 = 0; \qquad \mathscr{C}_2 = \underline{e}^{l\mathrm{T}}_2 \underline{e}^k_3 = 0; \qquad \mathscr{C}_3 = \underline{e}^{k\mathrm{T}}_3 (\underline{u}_0 + \underline{u}) = 0, \tag{2}$$

where $\underline{u}_0 = \underline{u}^\ell_0 - \underline{u}^k_0$ and $\underline{u} = \underline{u}^\ell - \underline{u}^k$. Kinematic condition $\mathscr{C}_3 = 0$ implies that body L remains in the plane normal to $\underline{e}^{k\mathrm{T}}_3$ and passing through body K. Conditions $\mathscr{C}_1 = \mathscr{C}_2 = 0$ imply that $\underline{e}^l_3$ remains normal to that same plane. The implementation of the holonomic constraints (Eq. (2)) is discussed in Bauchau (1998).

Contact may occur between the inner and outer races of the joint. As shown in Fig. 1, the relative distance q between the races is

$$q = \rho^k - \rho^\ell - |\underline{u}_0 + \underline{u}|. \tag{3}$$

This equation defines the relative distance q in terms of the kinematic variables of the planar joint. The relative distance is defined by the addition of a fourth constraint

$$\mathscr{C}_4 = q - \rho^k + \rho^\ell + |\underline{u}_0 + \underline{u}| = 0. \tag{4}$$

As discussed in Bauchau (1998), holonomic constraints are enforced by the addition of a constraint potential $\lambda\mathscr{C}$, where λ is the Lagrange multiplier. The forces of constraint $\underline{\mathscr{F}}^{\mathrm{c}}$ corresponding to this constraint are readily obtained as

$$\lambda\delta\mathscr{C} = \begin{bmatrix} \delta\underline{u}^k \\ \delta\underline{u}^\ell \\ \delta q \end{bmatrix}^{\mathrm{T}} \begin{bmatrix} -\lambda\underline{\Delta}/d \\ \lambda\underline{\Delta}/d \\ \lambda \end{bmatrix} = \begin{bmatrix} \delta\underline{u}^k \\ \delta\underline{u}^\ell \\ \delta q \end{bmatrix}^{\mathrm{T}} \underline{\mathscr{F}}^{\mathrm{c}}, \tag{5}$$

where $\underline{\Delta} = \underline{u}_0 + \underline{u}$, and $d = |\underline{\Delta}|$. The subscripts $(\cdot)_\mathrm{i}$ and $(\cdot)_\mathrm{f}$ denote the value of a quantity at the beginning and end times of a typical time step, denoted t_i and t_f, respectively. The change in the value of the constraint between the final and initial states is now evaluated

$$\mathscr{C}_{4\mathrm{f}} - \mathscr{C}_{4\mathrm{i}} = (q_\mathrm{f} - q_\mathrm{i}) + d_\mathrm{f} - d_\mathrm{i} = (q_\mathrm{f} - q_\mathrm{i}) + \frac{\underline{\Delta}_m^\mathrm{T}}{d_m}(\underline{u}_\mathrm{f} - \underline{u}_\mathrm{i}), \tag{6}$$

where the subscript $(\cdot)_m$ indicates an averaged quantity, i.e. $\underline{\Delta}_m = (\underline{\Delta}_\mathrm{f} + \underline{\Delta}_\mathrm{i})/2$ and $d_m = (d_\mathrm{f} + d_\mathrm{i})/2$. This result suggests the following time discretization of the constraint forces

$$\underline{\mathscr{F}}_m^\mathrm{c} = \begin{bmatrix} -s\lambda_m \underline{\Delta}_m/d_m \\ s\lambda_m \underline{\Delta}_m/d_m \\ s\lambda_m \end{bmatrix}, \tag{7}$$

where s is a scaling factor for the unknown, mid-point value of the Lagrange multiplier λ_m. In view of Eq. (6), the work done by the constraint forces during the time step is $\Delta\mathscr{W}^\mathrm{c} = s\lambda_m(\mathscr{C}_{4\mathrm{f}} - \mathscr{C}_{4\mathrm{i}})$. Clearly, this work vanishes if $\mathscr{C}_{4\mathrm{f}} - \mathscr{C}_{4\mathrm{i}} = 0$. In order to avoid the drift phenomenon, it is preferable to enforce the condition $\mathscr{C}_{4\mathrm{f}} = 0$ at each time step. Consequently, the forces of constraint are discretized in time in a manner that guarantees the satisfaction of the nonlinear constraint manifold, i.e. the constraint condition will not drift. At the same time, the discretization implies the vanishing of the work performed by the forces of constraint at the discrete solution level. As a result, the discrete energy conservation laws proved for the flexible members of the system are not upset by the introduction of the constraints. This energy preserving formulation can be readily extended to an energy decaying formulation by following the steps outlined in Section 4.3 of Bauchau (1998). The discretized forces of constraint (Eq. (7)) can be linearized to yield the Jacobian matrix of the constraints. Within the framework of the finite element formulation, this equivalent stiffness matrix is assembled with all other stiffness contributions of the system. The Lagrange multipliers are then explicitly computed at each time step.

The proposed formulation is also valid for a spherical joint with clearance. In this case, the displacements and rotations of body K and L are free, and constraint (4) is used to define the relative distance q.

3.2. Three-dimensional case: the spatial clearance joint

When the motion of the joint cannot be assumed to remain planar, a more complex, three-dimensional configuration must be considered, such as that presented in Fig. 2. The outer race of the joint, denoted body K, is idealized as a cylinder of radius ρ^k. The inner race, denoted body L, is idealized as a thin disk of radius ρ^ℓ. In the reference configuration, the position of the outer race is defined by the position vector $\underline{u}_0^k$ of its center and its orientation is determined by a body attached triad $\mathscr{S}_0^k$, with $\underline{e}_{30}^k$ along the axis of the cylinder. In the deformed configuration, the outer race center undergoes a displacement $\underline{u}^k$ and its orientation is defined by a triad $\mathscr{S}^k$. The kinematic variables associated with body L are defined in a similar manner, with $\underline{e}_{30}^l$ normal to the axis of the disk.

A triad $\underline{d}_1^k$, $\underline{d}_2^k$, $\underline{d}_3^k$ is now defined in the following manner: $\underline{d}_3^k = \underline{e}_3^k$ is along the axis of the cylinder, $\underline{d}_1^k$ makes an arbitrary angle ϕ with $\underline{e}_1^k$, and $\underline{d}_2^k$ completes the triad

$$\underline{d}_1^k = \cos\phi\,\underline{e}_1^k + \sin\phi\,\underline{e}_2^k; \qquad \underline{d}_2^k = -\sin\phi\,\underline{e}_1^k + \cos\phi\,\underline{e}_2^k; \qquad \underline{d}_3^k = \underline{d}_1^k \times \underline{d}_2^k. \tag{8}$$

Consider now the plane tangent to the cylinder, defined by vectors $\underline{d}_2^k$ and $\underline{d}_3^k$, as depicted in Fig. 3. Point P, of position vector $\underline{u}_0^k + \underline{u}^k + \rho^k \underline{d}_1^k$, belongs to this plane.

The relative distance $\bar{q}$ between disk L and this tangent plane is now evaluated. The candidate contact points on the plane and disk are denoted z^k and z^ℓ, respectively (see Fig. 3). The tangent to the disk at the candidate contact point must be in the plane of the disk and parallel to the contacting plane, i.e. normal to $\underline{e}_3^\ell$ and $\underline{e}_3^k$, respectively. The following triad is now defined

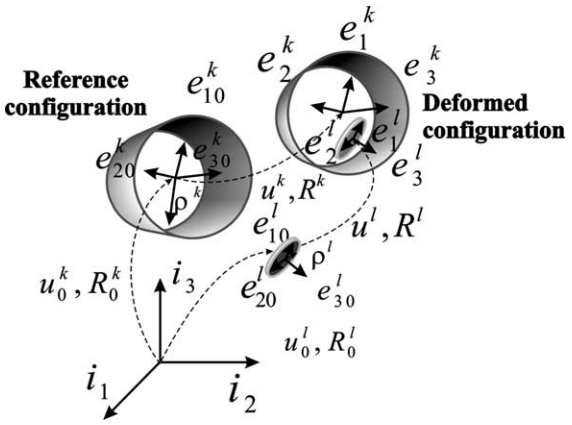

Fig. 2. Configuration of the spatial clearance element.

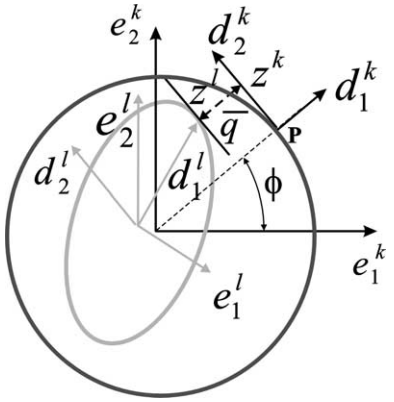

Fig. 3. Relative distance between the candidate contact points.

$$\underline{d}_2^\ell = -\frac{\widetilde{d}_1^k \underline{e}_3^\ell}{h}; \qquad \underline{d}_3^\ell = \underline{e}_3^\ell; \qquad \underline{d}_1^\ell = \widetilde{d}_2^\ell \underline{e}_3^\ell, \tag{9}$$

where $h = |\widetilde{d}_1^k \underline{e}_3^\ell|$. Clearly, $\underline{d}_2^\ell$ is parallel to the tangent at the candidate contact point, $\underline{d}_1^\ell$ points toward the candidate contact point, and $\underline{d}_3^\ell$ is normal to the plane of the disk. The vector from point P to point z^ℓ is

$$\underline{Pz}^\ell = \left[(\underline{u}_0^\ell + \underline{u}^\ell) + \rho^\ell \underline{d}_1^\ell\right] - \left[(\underline{u}_0^k + \underline{u}^k) + \rho^k \underline{d}_1^k\right] = \underline{u}_0 + \underline{u} + \rho^\ell \underline{d}_1^\ell - \rho^k \underline{d}_1^k, \tag{10}$$

where ρ^ℓ is the radius of the disk, $\underline{u}_0 = \underline{u}_0^\ell - \underline{u}_0^k$, and $\underline{u} = \underline{u}^\ell - \underline{u}^k$. The relative distance $\bar{q}$ is found by projecting $\underline{Pz}^\ell$ along the unit vector $-\underline{d}_1^k$ (see Fig. 3) to find

$$\bar{q} = -\underline{d}_1^{k\mathrm{T}} \underline{Pz}^\ell = -\underline{d}_1^{k\mathrm{T}} (\underline{u}_0 + \underline{u}) - \rho^\ell \underline{d}_1^{l\mathrm{T}} \underline{d}_1^k + \rho^k. \tag{11}$$

As shown in Fig. 3 the candidate contact point z^k is in the tangent plane, but not necessarily on the cylindrical surface defining the outer race of the joint. The relative distance $\bar{q}$ defined by Eq. (11) is clearly a function of the angle ϕ that defines the location of the tangent plane around the cylinder. The relative distance q between the cylinder and disk is found by minimizing $\bar{q}$ with respect to the choice of ϕ, i.e. by setting $\mathrm{d}\bar{q}/\mathrm{d}\phi = 0$ to find

$$\underline{d}_2^{k\mathrm{T}}\left[\rho^\ell \frac{g}{h}\underline{e}_3^\ell - (\underline{u}_0 + \underline{u})\right] = 0, \tag{12}$$

where $g = \underline{e}_3^{l\mathrm{T}}\underline{d}_1^k$. Note that for small angles $g \approx 0$ and $h \approx 1$. An alternate manner of determining the angle ϕ is to observe that the minimum relative distance is obtained when $\underline{Pz}^\ell$ is orthogonal to $\underline{d}_2^k$. In view of Eq. (10), this condition is

$$\underline{d}_2^{k\mathrm{T}}\underline{Pz}^\ell = \underline{d}_2^{k\mathrm{T}}\left[(\underline{u}_0 + \underline{u}) + \rho^\ell \underline{d}_1^\ell\right] = 0. \tag{13}$$

At first, this geometric condition appears to be different from that obtained from the minimization of $\bar{q}$ with respect to ϕ (Eq. (12)). However, the use of Eq. (9) and of standard vector identities implies

$$\underline{d}_2^{k\mathrm{T}}\underline{d}_1^l = -\frac{1}{h}\underline{d}_2^{k\mathrm{T}}\widetilde{\underline{d}_1^k}\underline{e}_3^l\underline{e}_3^l = -\frac{1}{h}\underline{d}_2^{k\mathrm{T}}\left[\widetilde{e}_3^l\widetilde{e}_3^l\underline{d}_1^k\right] = -\frac{1}{h}\underline{d}_2^{k\mathrm{T}}\left[g\underline{e}_3^l - \underline{d}_1^k\right] = -\frac{g}{h}\underline{d}_2^{k\mathrm{T}}\underline{e}_3^l. \tag{14}$$

Introducing this result into Eq. (13) yields the previously found condition (12).

In summary, the relative distance between the inner and outer races of the joint can be found by imposing the following constraint

$$\mathscr{C} = q - \rho^k + (\underline{u}_0 + \underline{u})^{\mathrm{T}}\underline{d}_1^k + \rho^\ell \underline{d}_1^{l\mathrm{T}}\underline{d}_1^k = 0, \tag{15}$$

and by using a Newton iteration method to find the contact angle ϕ defined by Eq. (12). These two relations implicitly define the relative distance q and the angular location ϕ of the candidate contact points. The resulting constraint forces and corresponding discretization can be obtained in a manner similar to that discussed in the previous section.

A realistic model of a journal bearing with clearance is obtained by using two spatial clearance joints connected by a rigid body, as depicted in Fig. 4. Care must be taken to constrain the motion of the journal along its axis to prevent the inner race from slipping out of the outer race. To that effect, the relative distance q in the axial direction is defined

$$q = (\underline{u}^l - \underline{u}^k)^{\mathrm{T}}\underline{e}_3^k. \tag{16}$$

The following holonomic constraint can be used to find q,

$$\mathscr{C} = q - (\underline{u}^l - \underline{u}^k)^{\mathrm{T}}\underline{e}_3^k. \tag{17}$$

The associated constraint forces and corresponding discretization can be obtained in a manner similar to that discussed in the previous section.

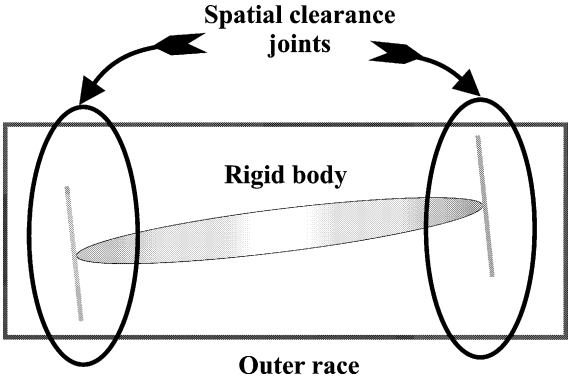

Fig. 4. The thin-disk/cylinder pair.

4. Unilateral contact condition

If the inner and outer races of the joint are assumed to be perfectly rigid, the unilateral contact condition is expressed by the inequality $q \geqslant 0$, where the relative distance is given by Eq. (4) or (15), for the two- and three-dimensional cases, respectively. This inequality constraint can be readily transformed into an equality constraint $q - r^2 = 0$ through the addition of a slack variable r. Hence, the unilateral contact condition is enforced as a nonlinear holonomic constraint

$$\mathscr{C} = q - r^2 = 0. \tag{18}$$

This constraint is enforced via the Lagrange multiplier technique discussed earlier.

In general, both inner and outer races of the joint will present local deformations in a small region near the contact point. In this case, the center of mass of the races are allowed to approach each other closer than what would be allowed for rigid races. This quantity is defined as the *approach* and is denoted a; following the convention used in the literature (see e.g. Timoshenko and Gere, 1961), $a > 0$ when penetration occurs. For the same situation, $q < 0$, see Eqs. (4) and (15). When no penetration occurs, $a = 0$, by definition, and $q > 0$. Combining the two situations leads to the contact condition $q + a \geqslant 0$, which implies $q = -a$ when penetration occurs. Here again, this inequality condition is transformed into an equality condition $\mathscr{C} = q + a - r^2 = 0$ by the addition of a slack variable r. This constraint is enforced via the Lagrange multiplier technique.

When the races are allowed to deform, a relationship between the contact force F and the approach must be selected. Hertz contact theory (see e.g. Timoshenko and Gere, 1961) states that $F = ka^{3/2}$ for the contact between two sphere; the stiffness constant k depends on the material properties and radii of the spheres in contact. For journal bearings, the inner and outer races are cylindrical, hence, this relationship is no longer valid. Dubowsky and Freudenstein (1971) suggest a force–displacement relationships of the form $a = k_1 F(\ln k_2 - \ln F)$, where k_1 and k_2 are constants that depend on the material properties and the geometry of the bearing. Similar or identical expressions are used by other authors (see e.g. Ravn et al., 1999; Liu and Lin, 1990; Rogers and Andrews, 1977).

5. Lubrication model

The pressure distribution in the oil film used to lubricate a bearing can be found by solving Reynolds equation (see e.g. Dowson and Higginson, 1966). The derivation of this equation requires a number of assumptions: incompressible, Newtonian fluid; uniform viscosity; laminar flow; constant pressure across the film thickness; and negligible body and inertial forces. If the pressure variation in the direction parallel to the journal is assumed to be negligible, closed form solutions can be found, as suggested by Pinkus and Sternlicht (1961). This corresponds to an infinitely long bearing with negligible end leakage effects. Fig. 5 shows the outer and inner races of a revolute joint with lubricant. The following triad is defined

$$\underline{d}_1 = \frac{\underline{u}}{|\underline{u}|}; \qquad \underline{d}_3 = \underline{e}_3^k; \qquad \underline{d}_2 = \widetilde{d}_3 \underline{d}_1, \tag{19}$$

where $\underline{u} = \underline{u}_0^l - \underline{u}_0^k + \underline{u}^l - \underline{u}^k$. Clearly, $\underline{d}_1$ defines the position for minimum film thickness h. The eccentricity e and its derivative $\dot{e}$ are defined as

$$e = |\underline{u}|; \qquad \dot{e} = \dot{\underline{u}}^{\mathrm{T}} \underline{d}_1, \tag{20}$$

or in nondimensional form

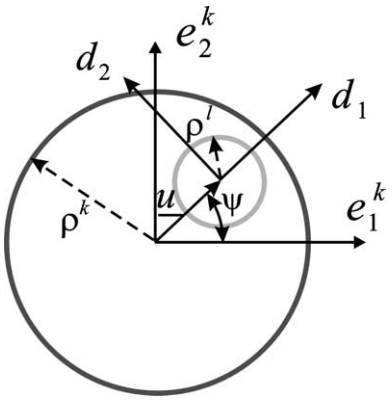

Fig. 5. Bearing with lubricant.

$$\epsilon = \frac{e}{\rho^k - \rho^l}; \qquad \dot{\epsilon} = \frac{\dot{e}}{\rho^k - \rho^l}. \tag{21}$$

The derivation of Pinkus and Sternlicht (1961) gives the forces F_1 and F_2 acting on the journal in the $\underline{e}_1^k$ and $\underline{e}_2^k$ directions, respectively, as

$$F_1 = -\frac{\mu L {\rho^l}^3}{(\rho^k - \rho^l)^2}\ (F_r \sin\psi - F_t \cos\psi); \qquad F_2 = \frac{\mu L {\rho^l}^3}{(\rho^k - \rho^l)^2}\ (F_r \cos\psi - F_t \sin\psi), \tag{22}$$

where L is the bearing length, and

$$F_r = \frac{6\pi\epsilon(\omega - 2\dot{\psi})}{(2+\epsilon^2)(1-\epsilon^2)^{1/2}} K; \qquad F_t = \frac{6\dot{\epsilon}}{(2+\epsilon^2)(1-\epsilon^2)^{3/2}} [4k\epsilon^2 + \pi(2+\epsilon^2)K]. \tag{23}$$

The parameters used in these expression are defined as

$$k^2 = (1-\epsilon^2)\left[\left(\frac{\omega - 2\dot{\psi}}{2\dot{\epsilon}}\right)^2 + \frac{1}{\epsilon^2}\right]; \tag{24}$$

$$K = \begin{cases} (k+3)/(k+3/2) & \dot{\epsilon} > 0 \\ k/(k+3/2) & \dot{\epsilon} < 0 \end{cases}; \tag{25}$$

and $\omega = (\underline{\omega}^l - \underline{\omega}^k)^{\mathrm{T}} \underline{e}_3^k$.

For the case of bearings of finite length, numerical solutions of Reynolds equation have been proposed in the literature for bearing lubrication applications (Liu and Lin, 1990). Such solutions could be used for the modeling of lubrication in spatial clearance joints.

6. Electrical motors

In multibody simulations, dynamical systems are often driven at a constant angular velocity by prescribing the relative rotation at a revolute joint. While this is a convenient approximation, it implies that unlimited power is available to obtain the desired rotation, resulting in an overly stiff system. When dealing with elastic systems, this unlimited power can excite very high frequency oscillations of the elastic

components, resulting in numerous intermittent contact events and high contact forces. Consequently, the modeling of structural damping appears to be indispensable for this type of problems.

In practice, drive trains have specific physical characteristics that couple with system dynamics and a realistic model of the drive system appears to be particularly important when dealing with clearance joints. To illustrate this point a simple model of a direct current (DC) motor will be used. For this drive system, an input voltage V and current I create an output torque T. The current is governed by the following differential equation

$$L\frac{\mathrm{d}I}{\mathrm{d}t} + RI + K_\omega \frac{\mathrm{d}\phi}{\mathrm{d}t} = V, \tag{26}$$

where L is the motor inductance, R its resistance, K_ω a voltage coefficient that represents an induced voltage $e_m = K_\omega \omega$, and ϕ the relative rotation. The resulting torque is given as $T = K_\mathrm{T} I$, where K_T is the torque coefficient.

7. Numerical examples

The proposed formulation will be validated with the help of different numerical examples involving the contact condition and lubrication for different types of joints with clearance.

7.1. Crank-slider mechanism with a planar revolute joint

The first example deals with the crank-slider mechanism depicted in Fig. 6. The crank is connected to both ground and arm by means of revolute joints. A torque is applied to the crank so as to achieve a constant angular velocity Ω, rotating through an angular displacement θ. The arm is connected to the slider by a revolute joint. Both crank and arm are flexible, homogenous beams.

The physical properties of the system were as follows: angular velocity $\Omega = 150$ rpm, crank length $l_\mathrm{c} = 0.25$ m, arm length $l_\mathrm{a} = 0.75$ m, slider mass $m = 40$ kg. The entire system is made of steel (Young's modulus $E = 190$ GPa, Poisson's ratio $v = 0.33$, and density $\rho = 7{,}850$ kg/m^3) with a rectangular cross-section of 30×10 mm for both the crank and the arm. Structural damping in the flexible components was modeled by viscous forces $\underline{F}_d^*$ proportional to the strain rates, $\underline{F}_d^* = \mu_s C^* \dot{\underline{e}}^*$, where μ_s is the damping coefficient, $\underline{e}^*$ the strains, and C^* the cross-sectional stiffness matrix. $\underline{F}_d^*$, $\underline{e}^*$, and C^* are all measured in a body attached coordinate system. The proportional damping coefficient was $\mu_s = 10^{-4}$ s. The crank and arm were each modeled using four cubic beam elements. Simulations were run for four complete revolutions of the crank to obtain a periodic solution of the problem. The figures below present the results for the third revolution, using θ as the crank angular position ($0 \leqslant \theta \leqslant 2\pi$). The computation used the strategy for adaptation of the time step size described in Bauchau (1998). Typically 500–750 time steps were required per revolution.

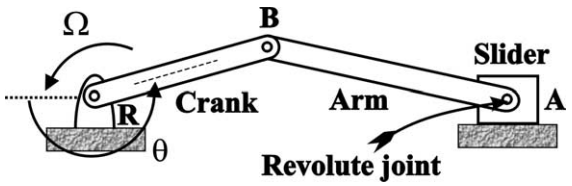

Fig. 6. Crank-slider mechanism.

Table 1
Physical properties of the motor

Motor constant	Value
Rated current	40 A
Rated power	15 hp
Nominal speed	150 rpm
No-load speed	155 rpm
Torque coefficient	17.80 V s
Voltage coefficient	14.70 V s
Resistance	0.15 Ω
Inductance	100 μH
DC Voltage	225 V

Five cases were considered, denoted case A1 through A5. Case A1 is the baseline case. In case A2, the revolute joint at point A was replaced by planar clearance joint of inner and outer radii $\rho^I = 9.5$ mm and $\rho^k = 10$ mm, respectively. The contact model used Hertz contact theory with a stiffness coefficient $k = 64$ MN/m$^{3/2}$. The joint had no lubrication. Lubrication was added for case A3; the lubricant had a viscosity of $\mu = 400$ cp and the bearing a length $L = 15$ mm. Finally, in cases A4 and A5, the crank was driven by a DC motor operating under a constant input voltage of 225 V, the other motor properties are listed in Table 1. Case A4 had a revolute joint at point A, whereas case A5 had a planar clearance joint without lubrication.

Fig. 7 shows the crank driving torque for the five different cases. The presence of clearance (cases A2 and A3) significantly alters the torque required to drive the mechanism. Subsequent to elastic deformations of the mechanism induced by contact events at the clearance, the driving torque presents oscillations at a frequency near the first natural bending frequency of the arm. This results in a 35% increase in maximum torque between cases A1 and A2 or A3. Note that cases A2 and A3 present very similar responses. This should be expected, since both Hertz contact model and lubrication model imply a very high stiffness at contact. Of course, Hertz model requires contact to occur before any stiffness appears, whereas the lubrication model introduces an increasing stiffness as the races are coming in closer proximity to each other. The presence of dissipative terms in the lubrication model seems to be of minor importance. When the mechanism is driven by a DC motor (case A4), a large reduction in required torque is observed (a 33%

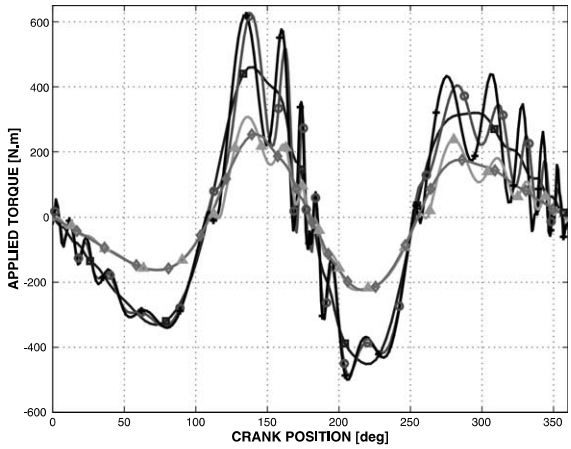

Fig. 7. Time history of the driving torque at the crank for cases A1: (□), A2: (+), A3: (○), A4: (◇), and A5: (△).

reduction from case A1 to A4). This is due to the fact that the crank is no longer rotating at a constant angular speed. The DC motor characteristics in Table 1 were selected so as to provide a nearly constant angular speed averaging 150 rpm over one revolution, (see Fig. 8). Case A5 features oscillations similar to those observed in cases A2 and A3, although the amplitudes are reduced; a 22% increase (from case A4 to A5) as compared to a 35% increase for cases A1 and A4. The arm mid-span bending moments are depicted in Fig. 9. The behavior of the various cases mirrors that observed in the previous figure. Finally, Fig. 10 shows the contact forces for cases A2 and A5. A large reduction (38% from case A2 to A5) in contact force is observed.

Next, elastic effects were investigated in cases B1 through B3. Case B1 is the baseline case, identical to case A2, whereas in cases B2 and B3 the stiffness characteristics of the system were artificially increased by multiplying Young's modulus 10 and 50 fold, respectively. Clearly, case B3 is a "nearly rigid" system. Fig. 11 shows the crank driving torque for the different cases. For cases B2 and B3, the oscillations observed at

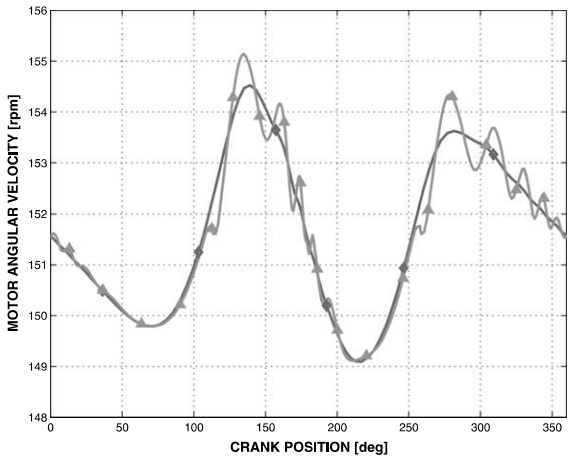

Fig. 8. Time history of the motor angular velocity for cases A4: (◇) and A5: (△).

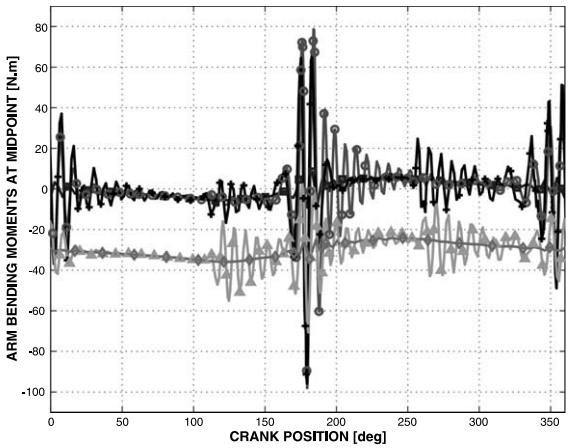

Fig. 9. Time history of the arm mid-span bending moments for cases A1: (□), A2: (+), A3: (○), A4: (◇), and A5: (△). For clarity, cases A4 and A5 were shifted down by 30 N m.

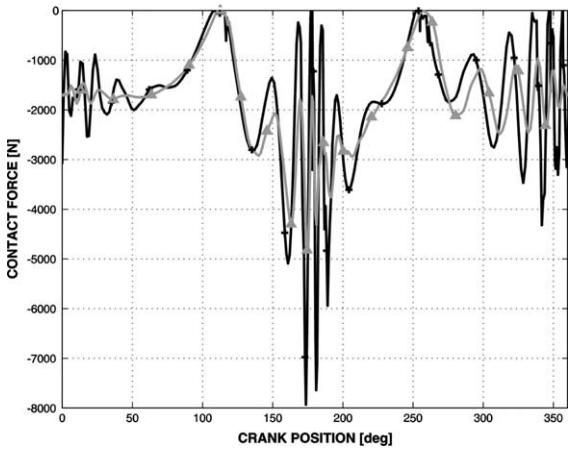

Fig. 10. Time history of the contact force for cases A2: (+) and A5: (△).

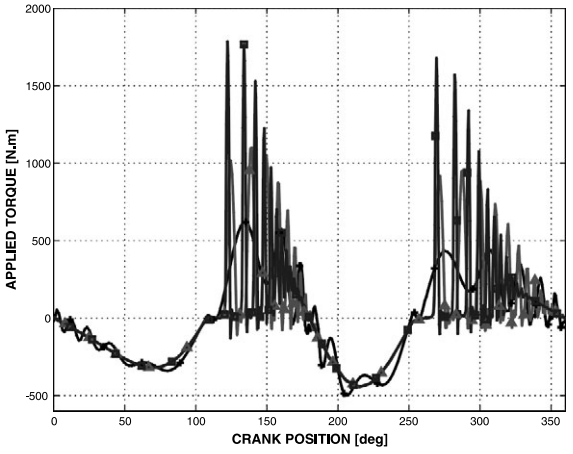

Fig. 11. Time history of the crank driving torque for case B1: (+); B2: (◇); B3: (□).

crank positions $\theta \approx 120°$ and 270° are replaced by oscillation of much shorter period (reflecting the increasing stiffness of the system) and much higher amplitude. The peak driving torque increased by about 77% and 190% for cases B2 and B3, respectively. The increased stiffness of the system also increased the number of contact events and the magnitude of the peak contact forces, as depicted in Fig. 12. It should be noted that the increasing stiffness of the system negatively impacts the computational time: cases B1 through B3 required about 800, 1000 and 1200 time steps per revolution, respectively.

Finally, the effect of structural damping in the arm and crank was investigated. Cases C1 through C4 are identical to case A1 but with proportional damping coefficients of $\mu_s = 10^{-3}$, 10^{-4}, 10^{-5} and 0 s, respectively. Cases C5 through C8 are identical to case case A2 with the same four values of proportional damping coefficients, respectively. Fig. 13 shows the crank driving torque for various cases, and illustrates the fact that the predicted response is rather insensitive to the magnitude of the damping coefficient. As expected, the oscillation amplitudes slightly increase as the damping coefficient is reduced. A similar behavior is observed for the arm mid-span bending moments depicted in Fig. 14, although the increase in

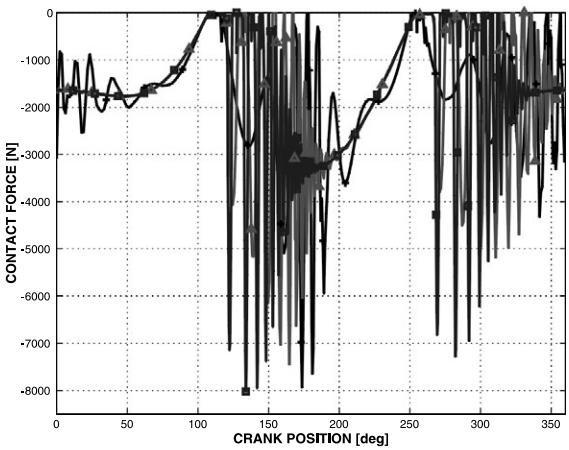

Fig. 12. Time history of the contact force for case B1: (+); B2: (◇); B3: (□).

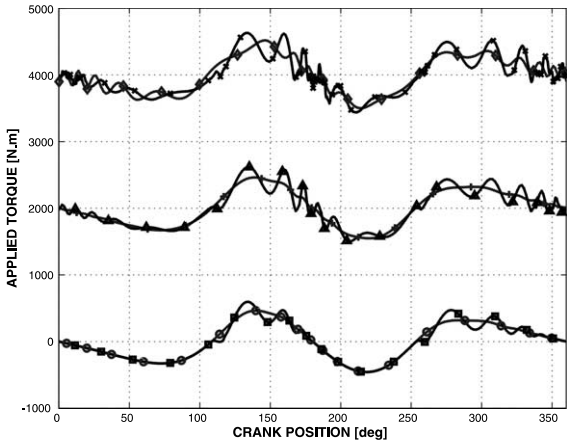

Fig. 13. Time history of the crank driving torque for case C1: (○); C2: (+); C3: (◇); C5: (□); C6: (△); C7: (×). For clarity, cases C2, C6 and C3, C7 were shifted up by 2000 and 4000 N m, respectively.

oscillation amplitude is significantly more pronounced as the damping coefficient is reduced. Fig. 15 shows the corresponding results for the contact force. Peak values of these forces are very sensitive to the damping coefficient; peak contact force increase 100% and 190% for $\mu_s = 10^{-4}$ and 10^{-5} s, respectively, when compared to the $\mu_s = 10^{-3}$ s case.

Fig. 16 illustrates the very high frequency oscillations that result from setting $\mu_s = 0$ s. Indeed, the very high vibration modes of the arm are excited at the first contact event and continue to vibrate in the absence of dissipation mechanisms. These high frequency oscillations then result in many more discrete contact events that in turns, increasingly excite high frequency modes. The predicted response in mainly high frequency "numerical noise", an artifact of the finite element discretization procedure, and bear little resemblance to the physical behavior of the system. Furthermore, the absence of dissipation mechanisms negatively impacts the computational process: baseline simulations ($\mu_s = 10^{-4}$ s) require about 600 time steps per revolution, simulations with clearance joints ($\mu_s = 10^{-4}$ s) about 800, and simulations with $\mu_s = 0$ s about 6000 steps. The effect of damping is much greater than the effect of lubrication (see Fig. 7). This

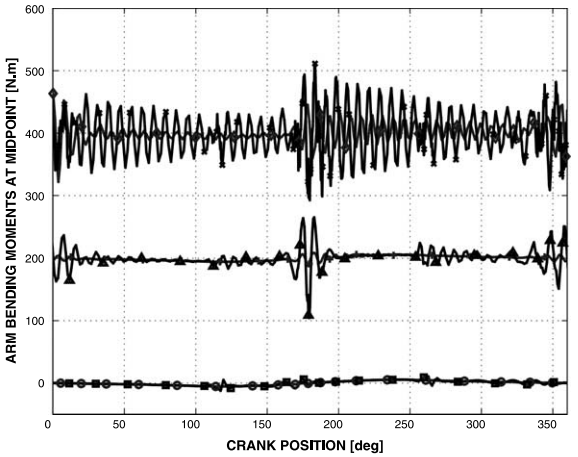

Fig. 14. Time history of the arm mid-span bending moments for case C1: (○); C2: (+); C3: (◇); C5: (□); C6: (△); C7: (×). For clarity, cases C2, C6 and C3, C7 were shifted up by 200 and 400 N m, respectively.

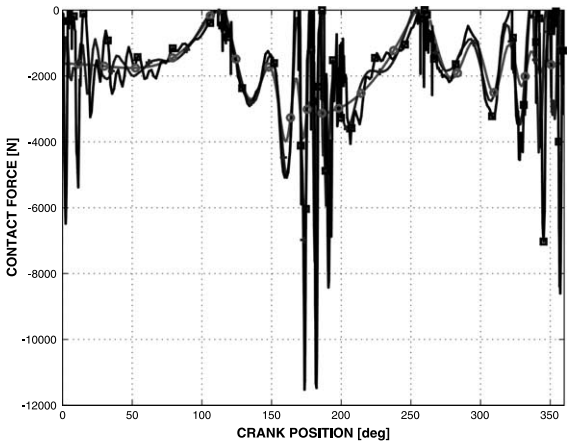

Fig. 15. Time history of the contact force for case C5: (○); C6: (+); C7: (□).

discussion leads to the following observations: an accurate evaluation of the importance of clearance effects requires the proper modeling of the elasticity of the system, a proper simulation of the drive system, and a precise knowledge of the dissipative forces present in the elastic mechanism. The impact of anyone of these phenomena is at least as important as the effect of joint clearance.

7.2. Crank-slider mechanism with a spatial clearance element

The second example deals with the crank-slider mechanism depicted in Fig. 17. The flexible mechanism is identical to that described in the first example. Three cases were considered, denoted case A1 through A3. Case A1 is the baseline case. In case A2 the revolute joint at point A was replaced by two spatial clearance joints of inner and outer radii $\rho^l = 9.5$ mm and $\rho^k = 10$ mm, respectively, joined by a rigid body. The

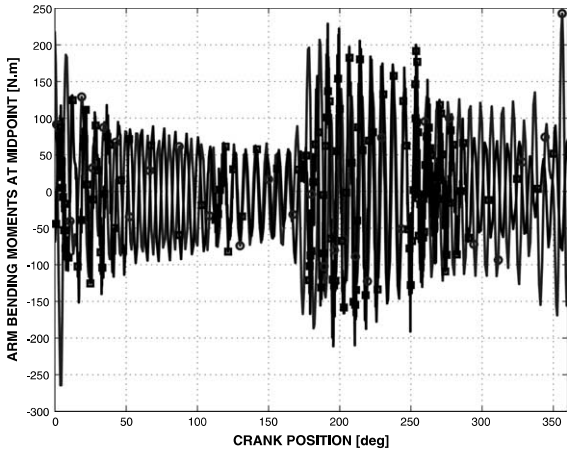

Fig. 16. Time history of the arm mid-span bending moments for case C4: (○) and case C8: (□).

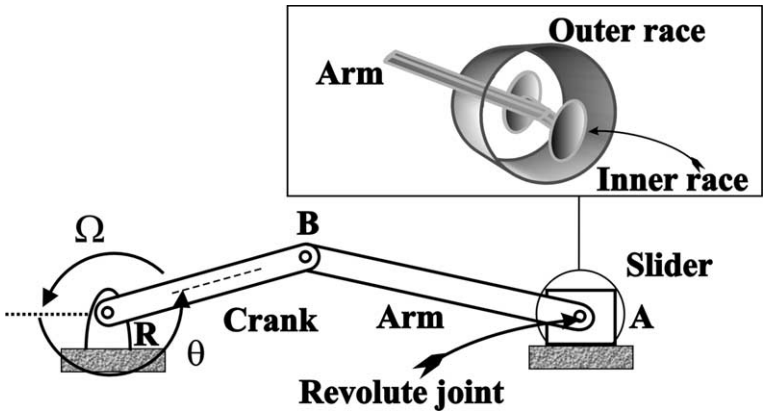

Fig. 17. Crank-slider mechanism with a spatial clearance element.

distance between the spatial clearance joints was $d = 15$ mm. The contact model for both joints used Hertz contact theory with a stiffness coefficient $k = 64$ MN/m$^{3/2}$. The joints had no lubrication. Finally, in case A3 the spatial clearance joint system was driven by a DC motor which properties are listed in Table 1. The presence of the spatial clearance joints profoundly alters the nature of the problem. Whereas for planar joints the position and orientation of the bearing inner race is constrained by Eq. (2), those same quantities are free for the spatial clearance joint. Hence, the inner race is free to undergo three dimensional displacements and rotations. The displacement of the inner race along its own axis was constrained by stops to ± 0.25 mm out-of-plane motions. Forces and moments are applied at the arm tip only when contact occurs at either of the spatial clearance joints. To demonstrate this effect, a short perturbation was applied at point B in the form of a triangular pulse of maximum amplitude of 10 N, and total duration of 0.3 s.

Fig. 18 shows the crank driving torque for the different cases. When compared to Fig. 7, it appears that the details of the clearance model had little effect on the torque required to drive the system. The arm out-of-plane tip displacements at point A (mid-point between the two spatial clearance joints) are shown in

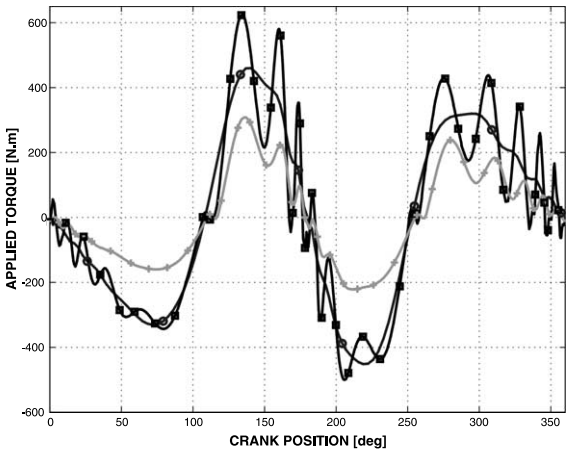

Fig. 18. Time history of the crank driving torque for case A1: (○), A2: (□), and A3: (+).

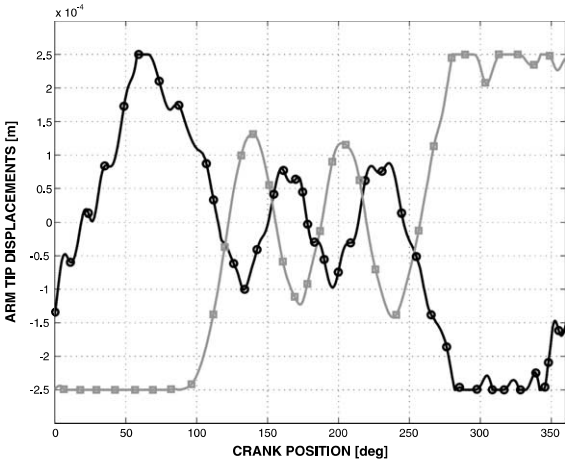

Fig. 19. Time history of the arm out-of-plane displacement at point A for case A2: (○), and A3: (□).

Fig. 19; of course, such displacements were zero for the previous example. In both cases A2 and A3, the inner race repeatedly hits the out-of-plane stops. Fig. 20 shows the contact forces in one of the two spatial clearance joints. Here again, lower contact forces (40% reduction from cases A2 and A3) are observed when the system is driven by a DC motor.

The three-dimensional nature of the system response raises questions about the stability of this flexible mechanism: Is there a critical angular speed above which the out-of-plane motion becomes unbounded? To investigate this problem, the out-of-plane stops were removed and the behavior of the system was studied for increasing crank speeds $\Omega = 75$, 126 and 150 rpm. Fig. 21 shows the out-of-plane arm displacements at point A. At low speed ($\Omega = 75$ rpm) the out-of-plane motion remains very small, whereas at high speed ($\Omega = 150$ rpm) the out-of-plane motion quickly diverges. The critical speed of $\Omega_{cr} = 126$ rpm was determined by trial and error: for speeds above Ω_{cr} the out-of-plane motion quickly diverges. The corresponding

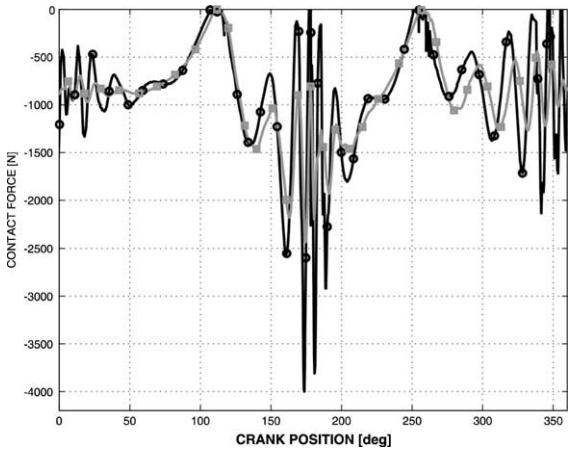

Fig. 20. Time history of the contact force for case A2: (○); case A3: (□).

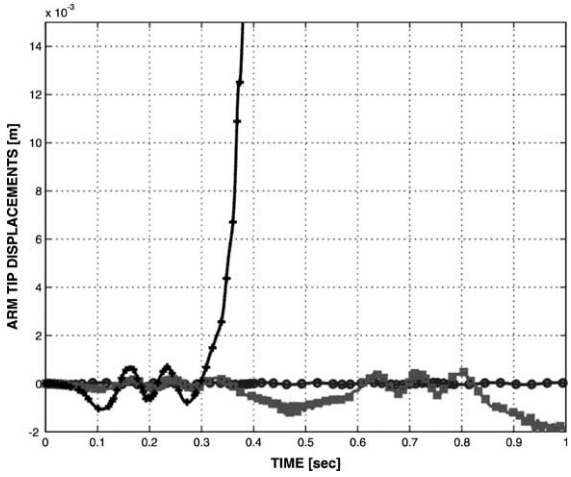

Fig. 21. Time history of the arm out-of-plane displacement at point A for $\Omega = 75$ rpm: (○), 126 rpm: (□), and 150 rpm: (+).

contact forces in the spatial clearance joint are shown in Fig. 22. As expected, these forces increase with increasing crank speed.

7.3. The quick return mechanism problem

The last numerical example is a classical quick return mechanism problem involving flexible bodies. Fig. 23 depicts the problem in the initial configuration: a flexible arm of length $L_a = 1.0$ m pivots about point B and is connected to a link of length $L_l = 0.25$ m. The link actuates the shuttle which is constrained by a prismatic joint to move in the horizontal direction only. A crank of length $L_c = 0.20$ m is pinned at R and slides along the arm. The formulation of sliding elements in flexible multibody systems can be found in Bauchau (2000); Bauchau and Bottasso (in press). A torque is applied to the crank so as to achieve an angular velocity Ω. Simulations were run for four complete revolutions of the crank to obtain a periodic solution of the problem. The figures below present the results for the third revolution.

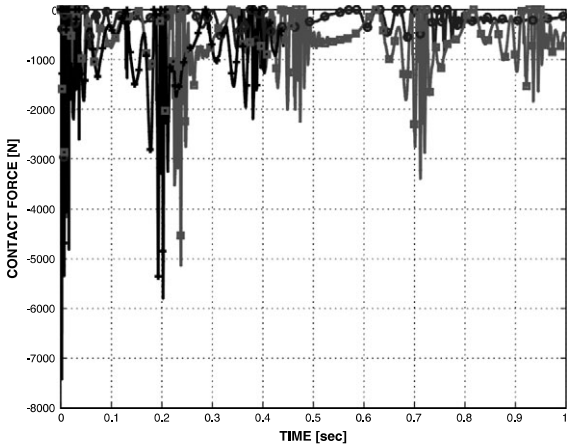

Fig. 22. Time history contact force for $\Omega = 75$ rpm: (○), 126 rpm: (□), and 150 rpm: (+).

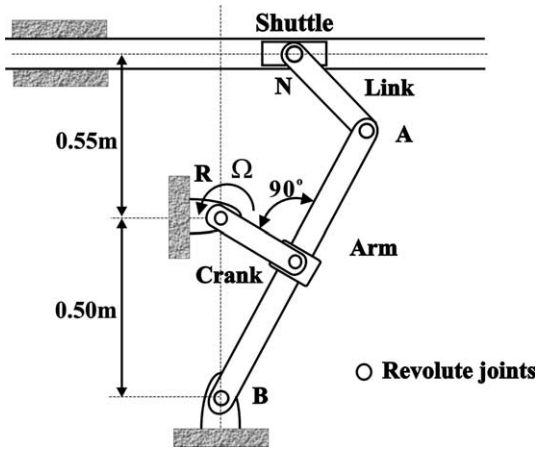

Fig. 23. The quick return mechanism problem.

Although modeled as flexible members by two cubic beam elements each, the crank and link were rather stiff linkages with the following physical properties: axial stiffness EA = 168.0 MN, bending stiffness EI = 5.0 MN m^2 shearing stiffness GK = 54.0 MN, mass per unit span $m = 6.16$ kg/m, and mass moment of inertia per unit span $I = 0.82$ g m^2. On the other hand, the arm was a flexible member modeled with 24 cubic elements, and had the following physical properties: axial stiffness EA = 168.0 MN, bending stiffness EI = 50.0 kN m^2, shearing stiffness GK = 54.0 MN, mass per unit span $m = 6.16$ kg/m, and mass moment of inertia per unit span $I = 2.1$ g m. The shuttle has a mass $M_s = 2.5$ kg and the sliding mechanism a mass $M_{sm} = 0.31$ kg and mass moment of inertia $I_{sm} = 0.27$ g m^2. The crank was driven by a DC motor presenting the characteristics listed in Table 1 which resulted in an average angular speed of $\Omega \approx 150$ rpm. The proportional damping coefficient was $\mu_s = 10^{-4}$ s for all flexible members of the system.

Three cases were investigated, denoted case 1 through 3. Case 1 is the baseline case corresponding to a rigid mechanism: the simulation was run with a very stiff arm (bending stiffness EI = 5.0 MN m^2). In case 2, the revolute joint at point N was replaced by a planar clearance joint of inner and outer radii $\rho^I = 9.5$ mm

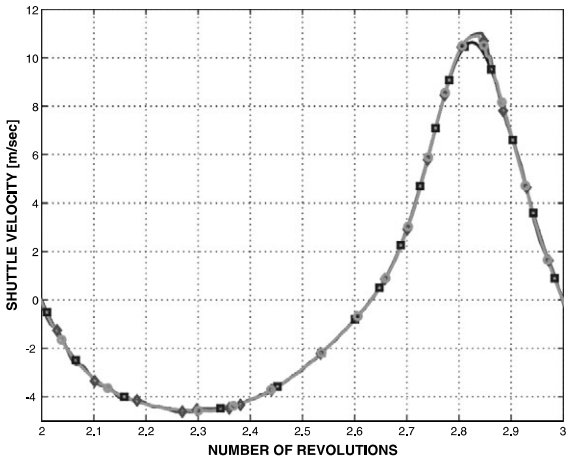

Fig. 24. Time history of the shuttle velocity for case 1: (□); case 2: (○); case 3: (◇).

and $\rho^k = 10$ mm, respectively. The contact model used Hertz contact theory with a stiffness coefficient $k = 64$ MN/m$^{3/2}$. Finally, case 3 involved two planar clearance joint at points N and B. No lubrication was used in the clearance joints.

Fig. 24 shows the time history of the shuttle velocity. As expected, the small joint clearance has little impact on system kinematics, and hence on shuttle velocity: a 4% increase is observed between cases 1 and 3. The arm quarter-point moments are more significantly altered, as shown in Fig. 25: the peak moment for case 3 is 34% higher than the baseline. The driving torque shown in Fig. 26 exhibits similar characteristics. The reason behind this increase in internal loads is the behavior of the contact forces at the joint clearance depicted in Fig. 27. For case 2, the history of the contact force is rather smooth, except during the latter part of the revolution (rev ≈ 2.8) when "knocking" is evident at the joint. A similar behavior is observed for case 3, although knocking is also observed in the early portion of the revolution, rev ≈ 2.2–2.4. As expected, the contact forces at point B are significantly larger, due to the configuration of the system. Finally, Fig. 28 shows the power required to drive the mechanism. As expected, cases 2 and 3 require more

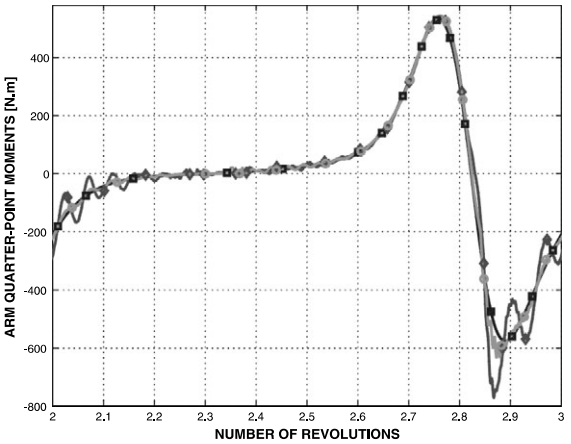

Fig. 25. Time history of arm quarter-point moments for case 1: (□); case 2: (○); case 3: (◇).

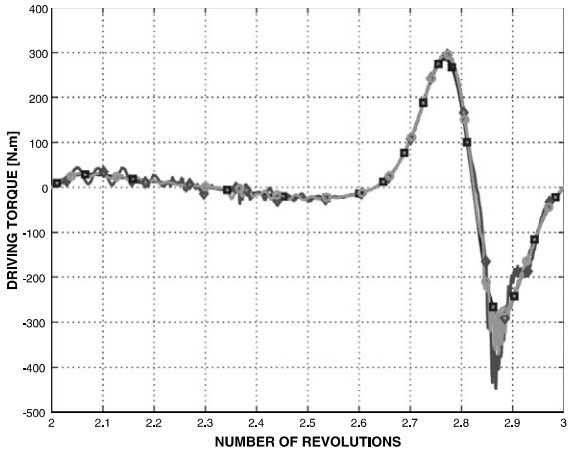

Fig. 26. Time history of the crank driving torque for case 1: (□); case 2: (○); case 3: (◇).

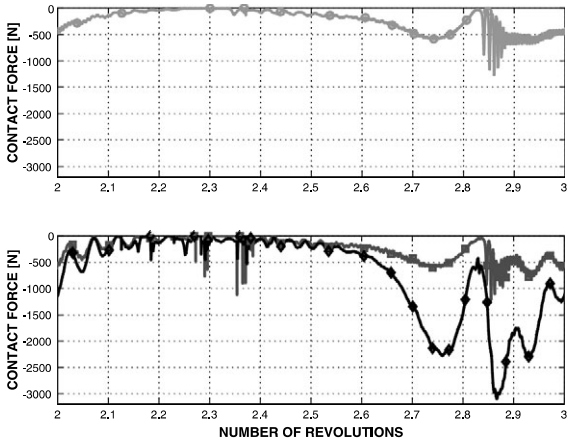

Fig. 27. Time history of the contact force for case 2 (top graph): point B (○); case 3 (bottom graph): point B (◇); point N (□).

instantaneous power: peak values are 33% and 66% higher for cases 2 and 3, respectively. This increased power is expended towards increasing the vibratory energy in the flexible mechanism. Repeated impacts at joint clearances are likely to increase wear and shorten the lifetime of the mechanism.

8. Conclusions

A comprehensive approach to the modeling of joints with clearance in nonlinear, flexible multibody systems has been presented. The problem was formulated within the framework of the finite element method and was conveniently broken into three distinct parts: a purely kinematic part describing the configuration of the joint inner and outer races, a unilateral contact condition giving rise to a contact force and a lubrication model. The formulation of these various aspects of the problem involved a number of

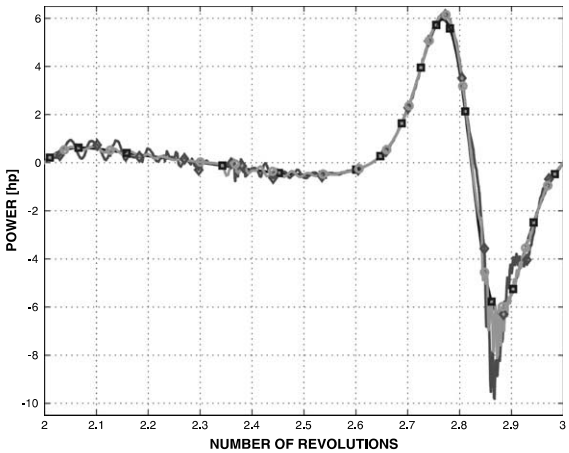

Fig. 28. Time history of the required power for case 1: (□); case 2: (○); case 3: (◇).

nonlinear holonomic constraints enforced via the Lagrange multiplier technique. This work was developed within the framework of energy preserving and decaying time integration schemes that provide unconditional stability for nonlinear, flexible multibody systems comprising joints with clearance.

The numerical examples presented in this paper leads to the following observations. An accurate evaluation of the importance of clearance effects requires the proper modeling of the elasticity of the system, a proper simulation of the drive system, and a precise knowledge of the dissipative forces present in the elastic mechanism. The impact of anyone of these phenomena is at least as important as the effect of joint clearance. When elasticity is neglected, peak forces are grossly overestimated. If the drive train is not properly modeled, peak forces are once again overestimated. Ignoring the effect of the dissipative forces in the elastic systems dramatically increases the computational cost, and generates large amounts of ''numerical noise''. In the presence of clearance, the effects of lubrication were found to be rather small in the sense that they had little impact on the overall dynamic response of the system.

Ignoring the effects of system compliance or material dissipative forces had a negative impact on computational efficiency as artificially small time step sizes were required to capture high frequency numerical noise. Finally, when appropriate models are used, the simulation of clearance in joints only results in a moderate increase of computational time (about 20–40%) as compared to the modeling of joints without clearance. Time step size adaptivity is an important part of the computational strategy.

References

Bauchau, O., 1998. Computational schemes for flexible, nonlinear multi-body systems. Multibody System Dynamics 2, 169–225.

Bauchau, O., 2000. On the modeling of prismatic joints in flexible multi-body systems. Computer Methods in Applied Mechanics and Engineering 181, 87–105.

Bauchau, O., Bottasso, C., 1999. On the design of energy preserving and decaying schemes for flexible, nonlinear multi-body systems. Computer Methods in Applied Mechanics and Engineering 169, 61–79.

Bauchau, O., Bottasso, C., 2000. Contact conditions for cylindrical, prismatic, and screw joints in flexible multi-body systems. Multibody System Dynamics 251–278.

Bauchau, O., Joo, T., 1999. Computational schemes for nonlinear elasto-dynamics. International Journal for Numerical Methods in Engineering 45, 693–719.

Bauchau, O., Theron, N., 1996a. Energy decaying scheme for non-linear beam models. Computer Methods in Applied Mechanics and Engineering 134, 37–56.

Bauchau, O., Theron, N., 1996b. Energy decaying schemes for nonlinear elastic multi-body systems. Computers and Structures 59, 317–331.

Bauchau, O., Damilano, G., Theron, N., 1995. Numerical integration of nonlinear elastic multi-body systems. International Journal for Numerical Methods in Engineering 38, 2727–2751.

Bengisu, M., Hidayetoglu, T., Akay, A., 1986. A theoretical and experimental investigation of contact loss in the clearances of a four-bar mechanism. Journal of Mechanisms, Transmissions and Automation in Design 108, 237–244.

Bottasso, C., Borri, M., 1997. Energy preserving/decaying schemes for non-linear beam dynamics using the helicoidal approximation. Computer Methods in Applied Mechanics and Engineering 143, 393–415.

Bottasso, C., Borri, M., 1998. Integrating finite rotations. Computer Methods in Applied Mechanics and Engineering 164, 307–331.

Bottasso, C., Borri, M., Trainelli, L., 2000. Integration of elastic multibody systems by invariant conserving/dissipating algorithms. Part I: formulation and Part II: numerical schemes and applications. Computer Methods in Applied Mechanics and Engineering 190, 3669–3733.

Cardona, A., Géradin, M., 1993. Kinematic and dynamic analysis of mechanisms with cams. Computer Methods in Applied Mechanics and Engineering 103, 115–134.

Deck, J., Dubowsky, S., 1994. On the limitations of predictions of the dynamic response of machines with clearance connections. Journal of Mechanical Design 116, 833–841.

Dowson, D., Higginson, G., 1966. Elasto-Hydrodynamic Lubrication. Pergamon Press, London.

Dubowsky, S., Freudenstein, F., 1971. Dynamic analysis of mechanical systems with clearances. Parts I and II. Journal of Engineering for Industry 93B, 305–316.

Dubowsky, S., Deck, J., Costello, H., 1987. The dynamic modeling of flexible spatial machine systems with clearance connections. Journal of Mechanisms, Transmissions and Automation in Design 109, 87–94.

Haines, R., 1980. Survey: 2-dimensional motion and impact at revolute joints. Mechanism and Machine Theory 15, 361–370.

Haug, E., Wehage, R., Barman, N., 1981. Design sensitivity analysis of planar mechanisms and machine dynamics. ASME Journal of Mechanical Design 103, 560–570.

Hunt, K., Crossley, F., 1975. Coefficient of restitution interpreted as damping in vibroimpact. Journal of Applied Mechanics 112, 440–445.

Kane, T., 1962. Impulsive motions. Journal of Applied Mechanics 15, 718–732.

Kane, T., 1968. Dynamics. Holt, Rinehart and Winston, New York.

Khulief, Y., Shabana, A., 1986. Dynamic analysis of constrained systems of rigid and flexible bodies with intermittent motion. ASME Journal of Mechanisms, Transmissions, and Automations in Design 108, 38–44.

Khulief, Y., Shabana, A., 1987. A continuous force model for the impact analysis of flexible multi-body systems. Mechanism and Machine Theory 22, 213–224.

Lankarani, H., Nikravesh, P., 1990. A contact force model with hysteresis damping for impact analysis of multi-body systems. Journal of Mechanical Design 112, 369–376.

Liu, T., Lin, Y., 1990. Dynamic analysis of flexible linkages with lubricated joints. Journal of Sound and Vibration 141, 193–205.

Pfeiffer, F., Glocker, C., 1996. Multi-Body Dynamics with Unilateral Contacts. Wiley, New York.

Pinkus, O., Sternlicht, S., 1961. Theory of Hydrodynamic Lubrication. McGraw-Hill, New York.

Ravn, P., Shivaswamy, S., Lankarani, H., 1999. Treatment of lubrication in long bearings for joint clearances in multibody mechanical systems. Proceedings of the ASME Design Technical Conference, Las Vegas, NV, September 12–15.

Rhee, J., Akay, A., 1996. Dynamic response of a revolute joint with clearance. Mechanism and Machine Theory 31, 121–134.

Rogers, R., Andrews, G., 1977. Dynamic simulation of planar mechanical systems with lubricated bearings clearances using vector-network methods. Journal of Engineering for Industry 99B, 131–137.

Simo, J., Tarnow, N., 1992. The discrete energy-momentum method. Conserving algorithms for nonlinear dynamics. ZAMP 43, 757–792.

Simo, J., Tarnow, N., 1994. A new energy and momentum conserving algorithm for the nonlinear dynamics of shells. International Journal for Numerical Methods in Engineering 37, 2527–2549.

Simo, J., Wong, K., 1991. Unconditionally stable algorithms for rigid body dynamics that exactly preserve energy and momentum. International Journal for Numerical Methods in Engineering 31, 19–52.

Simo, J., Tarnow, N., Doblare, M., 1995. Non-linear dynamics of three-dimensional rods: Exact energy and momentum conserving algorithms. International Journal of Numerical Methods in Engineering 38, 1431–1473.

Timoshenko, S., Gere, J., 1961. Theory of Elastic Stability. McGraw-Hill, New York.

Xie, H., Flowers, G., Feng, L., Lawrence, C., 1999. Steady-state dynamic behavior of a flexible rotor with auxiliary support from a clearance bearing. Journal of Vibration and Acoustics 121, 78–83.

Zakhariev, E., 1999. Dynamics of rigid multibody systems with clearances in the joints. Mechanisms, Structures and Machines 27, 63–87.